Stabilizing Ru Single Atom Catalyst Through Electronic Metal-Support Interaction with $NiCo_2O_4$ Support for Overall Water Splitting and Urea Electrolysis

Astha Gupta[a], Swarup Ghosh[b], Dinesh Bhalothia[c], Sadhasivam Thangarasu[d], Biplab Ghosh[e], Rajashri Urkude[e], Joydeep Chowdhury[b], and Surojit Pande[a*]

[a]Department of Chemistry, Birla Institute of Technology and Science, Pilani, Rajasthan-333031, India

E-mail: spande@pilani.bits-pilani.ac.in

[b]Department of Physics, Jadavpur University, 188, Raja S.C. Mallick Road, Kolkata, 700032, India. E-mail: joydeep.chowdhury@jadavpuruniversity.in

[c]Department of Engineering and System Science, NTHU, Taiwan

[d]School of Chemical Engineering, Yeungnam University, Gyeongsan 38541, Republic of Korea

[e]Beamline Development and Application Section, Bhabha Atomic Research Centre, Mumbai – 400085

Characterization of material: Powder X-ray diffraction (PXRD) was done using the Rikagu Mini Flex II diffractometer having incident radiation of Cu Kα. The data was recorded at 2º per min scan rate, from 10º to 80º for all the bare and doped samples. The morphology of the bare and doped $Ni_{0.85}Se$ material was inspected by field emission scanning electron microscopy (FESEM) instrument, model-"APREO S", XT microscope. Morphology, lattice spacing, and crystallinity were further examined with Field emission transmission electron microscope (FE-TEM, JEM-2100F). For TEM analysis, the samples were collected from carbon cloth via sonication and drop casted on a carbon-coated Cu grid and dried in a vacuum chamber. X-ray photoelectron spectroscopy (XPS) was performed with Omicron EA 125 source using Al Kα radiation having energy 1486.7 eV. Throughout the XPS analysis, base pressure was sustained < 10^{-9} m bar in the UHV. The HAADF-STEM images were collected at the National Sun Yat-sen University, Taiwan. The preparation of STEM samples began with dispersing the catalyst powder in isopropanol (IPA) through ultrasonication. This dispersion was then drop-cast onto 200 mesh copper grids. Afterward, the specimens were dried at 120°C for 48 hours in an oven. Before loading the samples into the TEM chamber, they were cleaned with plasma to remove any surface contaminants. As a reference, the binding energy peak at 284.5 eV of C 1s was used to detect any kind of variation. For electrochemical water splitting application, the CH instrument (CHI604E) was used. ICP analysis was done with model Perkin Elmer AVIO ICP spectrometer.

The K-edges of Ru (22117 eV), Ni (8333 eV) and Co (7709 eV), X-ray Near-Edge Structure (XANES) and Extended X-ray Absorption Fine Structure (EXAFS) measurements were performed at the Indus-2 Synchrotron Source's Energy-Scanning EXAFS beamline (BL-9) at the Raja Ramanna Centre for Advanced Technology (RRCAT), Indore, India. All measurements were taken at room temperature. The beamline optics are made up of a collimating meridional cylindrical mirror coated in Rh/Pt, and the collimated beam reflected by the mirror is monochromatized by a Si (111) based double crystal monochromator (DCM) for energy selection. The DCM's second crystal is a sagittal cylindrical crystal that is used for horizontal beam focusing, while another Rh/Pt coated bendable post mirror facing downward is used for vertical beam focusing at the sample position. To get a significant edge jump at the absorption edge of the element to be analysed, calculations were done. Calculated amount of sample then mixed with cellulose powder in proper amount and pressed (2 Ton) into a 1 mm diameter disc to made pellets. These pellets were used for recording absorption spectra. The data was

collected when the synchrotron source 2.5 GeV ring was operated at 120 mA injection current. XAFS (XANES and EXAFS) measurements were carried out in transmission and fluorescence mode. The ion chambers were filled with N2, He, and Ar for Ru, Ni and Co foils and for the samples. The second crystal of the monochromator was 60% detuned during the data collection to suppress the higher harmonic components. The energy calibration was performed using the Ru, Ni and Co metal foils as a reference. The standard normalization and background subtraction procedures were executed using the ATHENA software version 0.9.26 to obtain normalized XANES spectra.[1] Fourier transformed (FT) of EXAFS oscillations were calculated to observe the $|\chi(R)|$ vs R space spectra and its fitting was done using ARTEMIS software version 0.9.26 which uses FEFF6 and ATOMS programs to simulate the theoretical scattering paths according to crystallographic structure.[2]

Calculation Method

Electrochemical calculation:

The calculation of catalyst loading and mass activity of the electrocatalysts on carbon cloth was carried out using the following equations 1 and 2, respectively.

$$M_{catalyst} = \text{Weight}_{(\text{catalyst loaded CC})} - \text{Weight}_{(\text{Bare CC})} / \text{area (cm}^2\text{)} \quad [1]$$

$$\text{Mass activity} = \text{observed current density at a fixed potential/catalyst loading} \quad [2]$$

As a result, catalyst loading on carbon cloth was 0.25 mg on a 0.16 cm^2 area. Mass activity (A/g) for HER was calculated by using the observed current density at a fixed potential of -0.4 V *vs.* RHE. Mass activity (A/g) for OER was calculated by using the observed current density at a fixed potential of 1.65 V *vs.* RHE. To calculate the electrochemical surface-active area (ECSA) for OER, CV analysis was carried out at different scan rates and a fixed potential of 1.125 V *vs.* RHE, the observed current was plotted against the scan rate.

The slope of the observed straight line is the double-layer capacitance (C_{dl}), which is directly proportional to ECSA. To calculate the roughness factor, the ECSA of that electrode was divided by geometric area.

Tafel slope calculation, $\eta = a + b\log j$, where, "η" is the overpotential, "j" is the current density and "b" is the Tafel slope.

To determine the possible mechanism of HER, the following processes are known.

$$H_2O + e \longrightarrow H_{ads} + OH^- \text{ (Volmer), 120 mV/dec} \quad \text{and}$$
$$H_{ads} + H_{ads} \longrightarrow H_2 \text{ (Tafel), 30 mV/dec} \qquad [1]$$

$$H_2O + e \longrightarrow H_{ads} + OH^- \text{ (Volmer), 120 mV/dec} \quad \text{and}$$
$$H_2O + H_{ads} + e \longrightarrow H_2 + OH^- \text{ (Heyrovsky), 40 mV/dec} \qquad [2]$$

Preparation of standard electrocatalyst for HER and OER:

For the standard catalyst of HER and OER, 5% Pt/C and RuO_2 were used, respectively. The same amount of catalyst (0.25 mg) was used to compare the electrocatalytic activity. In a small glass vial, 0.25 mg of 5% Pt/C was taken along with 200 µL of isopropyl alcohol and 20 µL of Nafion (an adhesive), and the mixture was sonicated for 30 min. After that, the whole mixture was transferred quantitatively into 0.4×0.4 cm^2 CC and was used for HER. For OER same process was followed except RuO_2 was used instead of 5% Pt/C.

Urea electrolysis

The urea electrolysis involves two half-cell reactions and requires a theoretical cell voltage of 0.37 V to carry out the overall reaction.

$$\text{Anode: } CO(NH_2)_2 + 6OH^- \rightarrow CO_2 + N_2 + 5H_2O + 6e^- \text{ (E = -0.46 V } \textit{vs.} \text{ SHE)}$$

$$\text{Cathode: } 6H_2O + 6e^- \rightarrow 3H_2 + 6^-OH \text{ (E = -0.83 V } \textit{vs.} \text{ SHE)}$$

$$\text{Overall: } CO(NH_2)_2 + H_2O \rightarrow CO_2 + N_2 + 3H_2$$

Table S1: ICP-AES analysis of Ru-SAC $NiCo_2O_4$ sample.

ICP-OES	Ni (wt%)	Co (wt%)	Ru (wt%)
Ru-SAC $NiCo_2O_4$	12.6	26	2.03

Table S2: XAS determined quantitative structural parameters of the Ru-SAC $NiCo_2O_4$ and control samples.

Sample	Ru K-edge			Ni K-edge			Co K-edge		
	bond pair	CN	R	bond pair	CN	R	bond pair	CN	R
Ru-SAC $NiCo_2O_4$	Ru-Ru	N/A	N/A	Ni-Ni	6.13	2.894	Co-Co	3.98	2.945
	Ru-Ni	6.83	2.943	Ni-Ru	2.03	3.105	Co-Ru	2.34	2.910
	Ru-Co	5.26	2.962	Ni-Co	6.07	2.968	Co-Ni	6.02	2.987
	Ru-O	2.10	1.943	Ni-O	4.90	2.276	Co-O	5.13	2.289
$NiCo_2O_4$				Ni-Ni	6.03	2.893	Co-Co	4.01	2.943
		N/A		Ni-Co	5.99	2.963	Co-Ni	6.12	2.986
				Ni-O	4.86	2.268	Co-O	5.15	2.291

Table S3: XPS binding energy values of $NiCo_2O_4$, Ru-SAC $NiCo_2O_4$ (pre and post electrocatalysis)

Binding energy (eV)	**$NiCo_2O_4$**	**Ru-SAC $NiCo_2O_4$**	**Ru-SAC $NiCo_2O_4$ (Post electrolysis)**
Ni^{+2} ($2p_{3/2}$)	855.93	855.81	855.66
Ni^{3+} ($2p_{3/2}$)	854.21	854.09	853.95
Ni^{+2} ($2p_{1/2}$)	873.6	873.71	873.75
Ni^{+3} ($2p_{1/2}$)	872.07	872.08	871.99
Co^{+2} ($2p_{3/2}$)	781.44	781.57	781.47
Co^{+3} ($2p_{3/2}$)	779.82	779.75	779.66
Co^{+2} ($2p_{1/2}$)	796.63	796.65	796.48
Co^{+3} ($2p_{1/2}$)	794.93	794.86	794.72
O1	530	529.5	529.48
O2	531.5	531.13	531.17
O3	532.92	533.09	533.05
Ru ($2p_{3/2}$)		463.74	463.7
Ru ($2p_{1/2}$)		486.00	486.13

Table S4: A benchmark table comparing the performance with the literature for HER, OER, and two-electrode system

S. No.	Electrocatalyst	Electrolyte	Electrode Reaction	Potential (mV vs. RHE)	Tafel slope (mV/dec)	Stability	Ref
1.	Ru/Co_3O_{4-x}	1 M KOH	OER	280 at 10 mA/cm^2	86.9	150 h	4
2.	Ru/CoFe-LDHs	1 M KOH	OER	195 mV at 10 mA/cm^2	39	25 h	5
3.	(Ir−$NiCo_2O_4$NSs)	0.5 M H_2SO_4	OER	240 at 10 mA/cm^2	60	70 h	6
4.	$Ir_{0.06}Co_{2.94}O_4$	0.1 M $HClO_4$	OER	220 at 10 mA/cm^2	45	200 h	7
5.	Ru-MoS_2/CC	0.1 M H_2SO_4	HER	171 at 100 mA/cm^2	114	10 h	8
6.	Pt1/NMHCS	0.5 M	HER	40 at 10 mA/cm^2	56.66	10 h	9
7.	Co@CMB-N4	0.1 M KOH	Overall water splitting	1.59 V (Cell Potential) at 10 mA/cm^2		100 h	10
8.	$Pt_1/Co(OH)_2$	1 M KOH	Overall water splitting	1.48 V (Cell Potential) at 10 mA/cm^2		50 h	11
9.	Ru-SAC $NiCo_2O_4$	1 M KOH	Overall water splitting	1.57 V (Cell Potential) at 10 mA/cm^2		60 h	This work

Table S5: All HER parameters of $NiCo_2O_4$ and Ru-SAC $NiCo_2O_4$ samples

Electrode	**Potential (V) vs. RHE required to generate 10 mA/cm²**	**Tafel slope (mV/dec)**	**ECSA (cm²)**	**Mass Activity (A/g) at -04 V vs. RHE**	**R_f**	**R_s (Ohm)**	**R_{CT} (Ohm)**
$NiCo_2O_4$	-0.332 V	106.46	4	1.61	25	5.2	26.93
Ru-SAC $NiCo_2O_4$	-0.075 V	74.44	33.63	53.54	210.18	4.6	11.91
Pt/C (5%)	-0.02 V	68.88		79.16			

Table S6: All OER parameters of $NiCo_2O_4$ and Ru-SAC $NiCo_2O_4$ samples

Electrode	**Potential (V) vs. RHE required to generate 10 mA/cm2**	**Tafel slope (mV/dec)**	**Mass Activity (A/g) at 1.65 V vs. RHE**	**R_s (Ohm)**	**R_{CT} (Ohm)**
$NiCo_2O_4$	1.578 V	88.92	29.22	9.93	10.03
Ru-SAC $NiCo_2O_4$	1.511 V	79.08	73.54	5.24	4.14
RuO_2	1.617 V	176.66	9.03		

Figure S1: XRD analysis of metal-carbonate hydroxide complex, $(Ni_{1/3}Co_{2/3})_6(CO_3)_x(OH)_y.H_2O$.

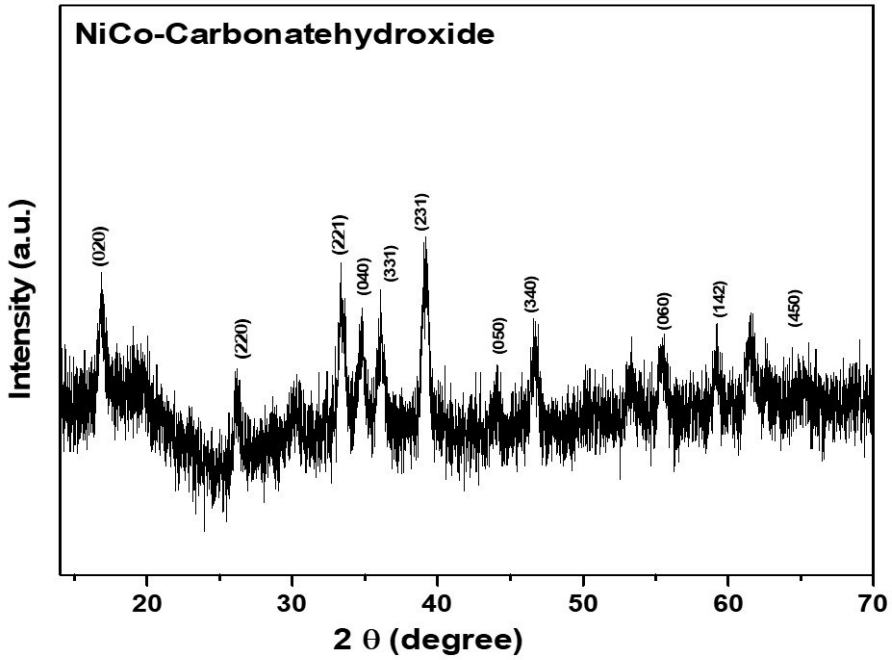

In the XRD pattern all the peaks are well collaborated with the existing literature.[3]

Figure S2: XRD analysis of pristine $NiCo_2O_4$ and Ru-SAC $NiCo_2O_4$

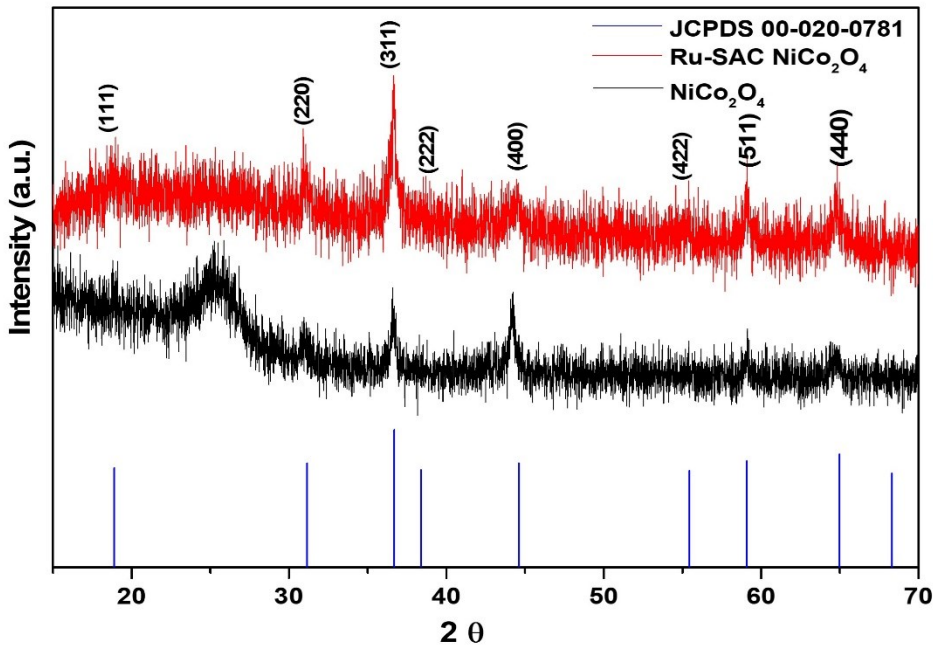

Figure S3: FESEM analysis of pristine $NiCo_2O_4$ sample at (a) low, (b) high magnification

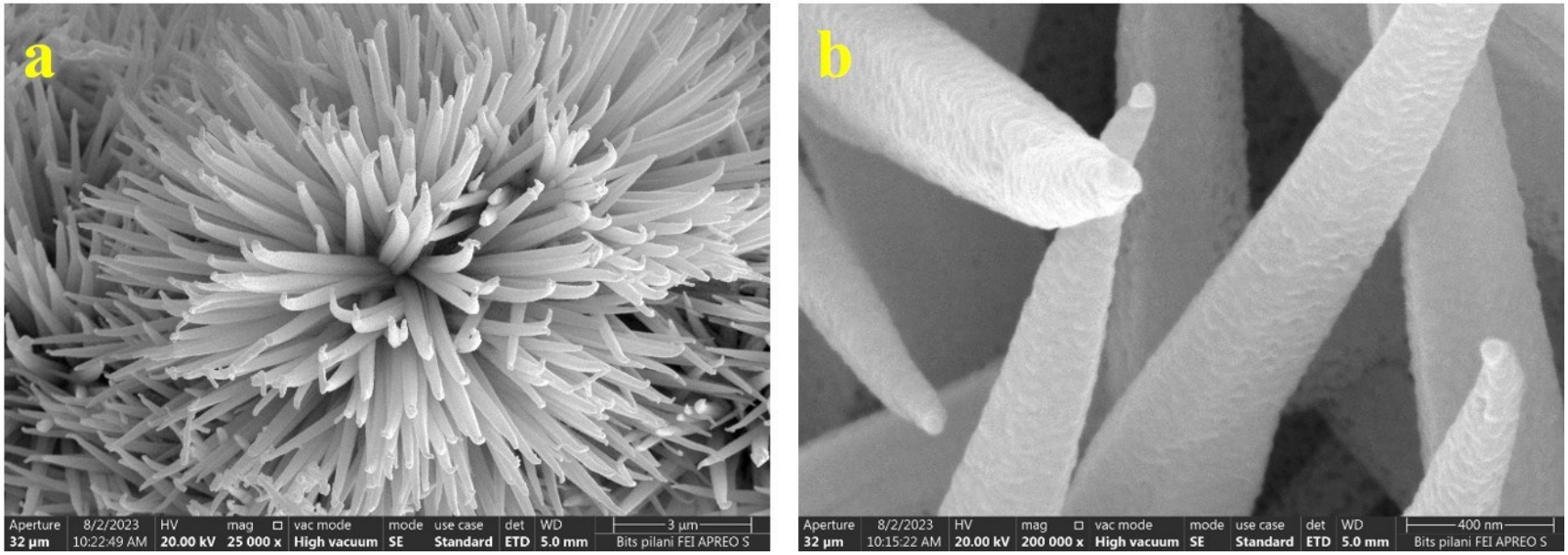

Figure S4: (a and b) TEM analysis of pristine $NiCo_2O_4$ at different magnifications.

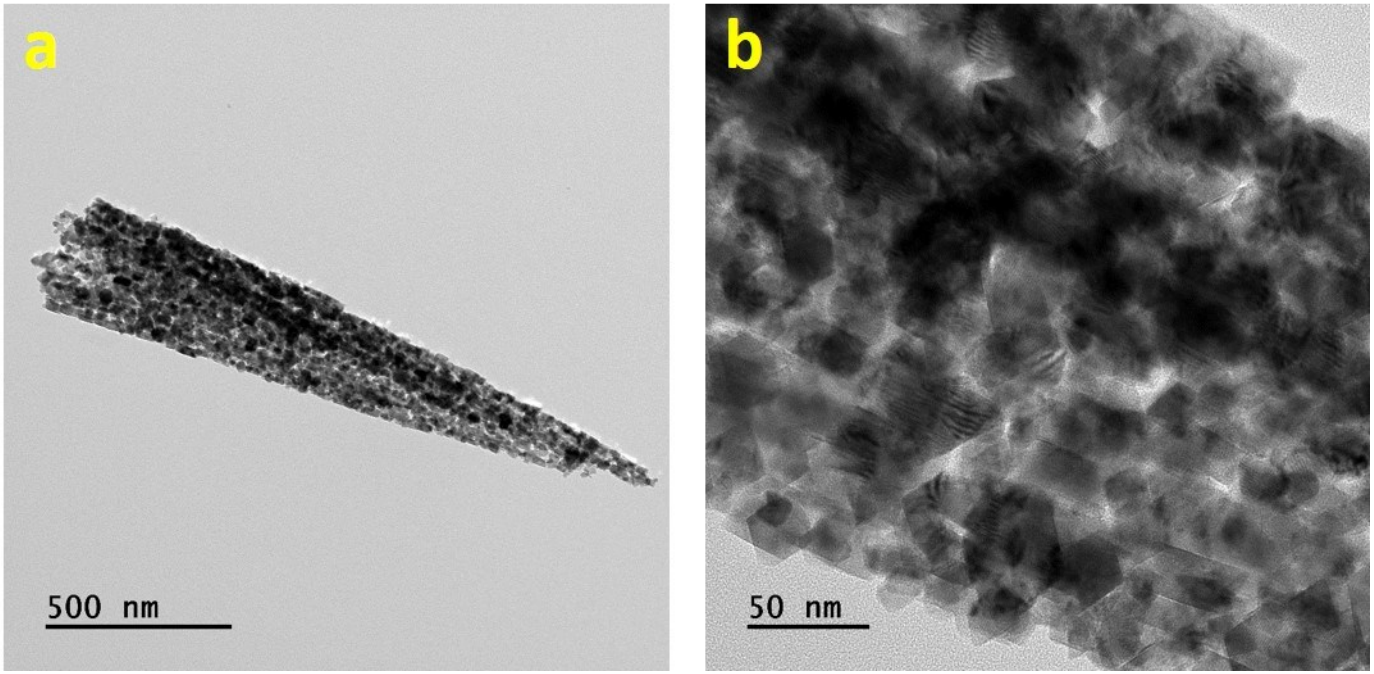

Figure S5: The overlay fitting curves of EXAFS spectra and model simulated fitting spectra.

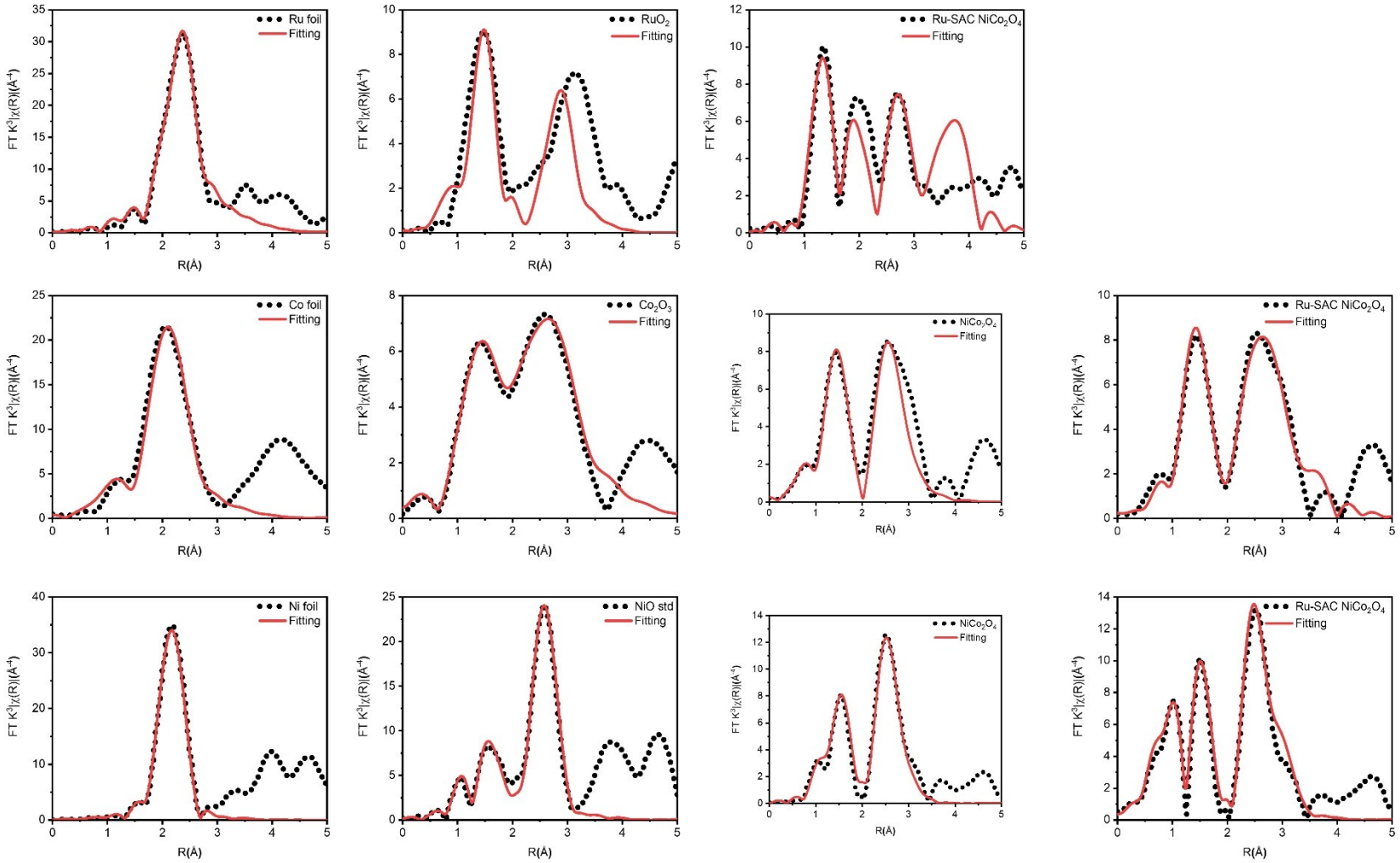

Figure S6: The k-space curves of experimental samples at (a) Ru K-edge, (b) Ni K-edge and (c) Co K-edge.

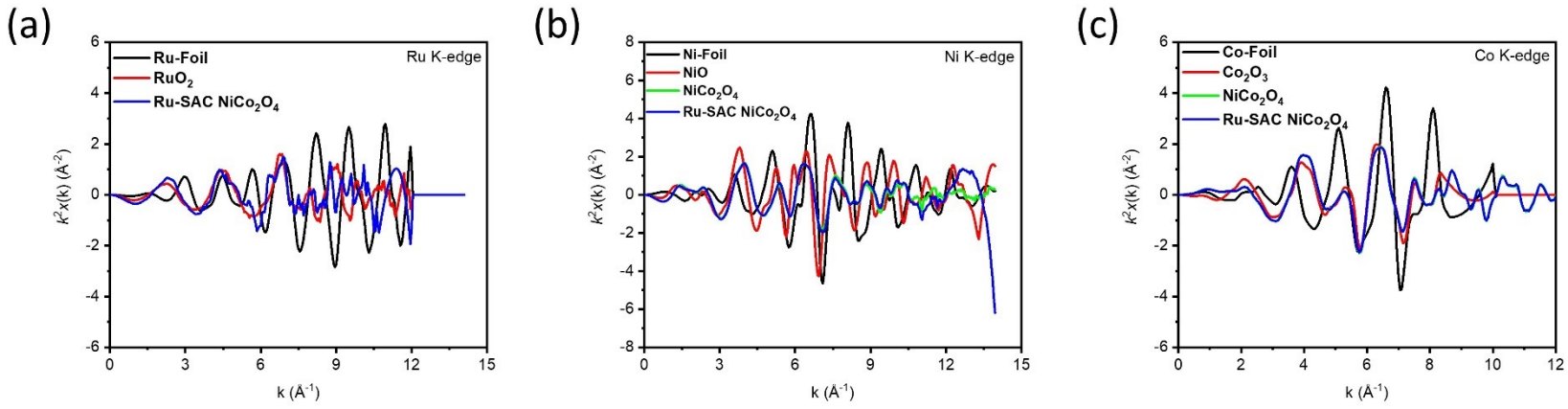

Figure S7: XPS analysis of $NiCo_2O_4$ (a) survey spectra, deconvoluted spectra of (b) Ni 2p, (c) Co 2p, and (d) O 1s

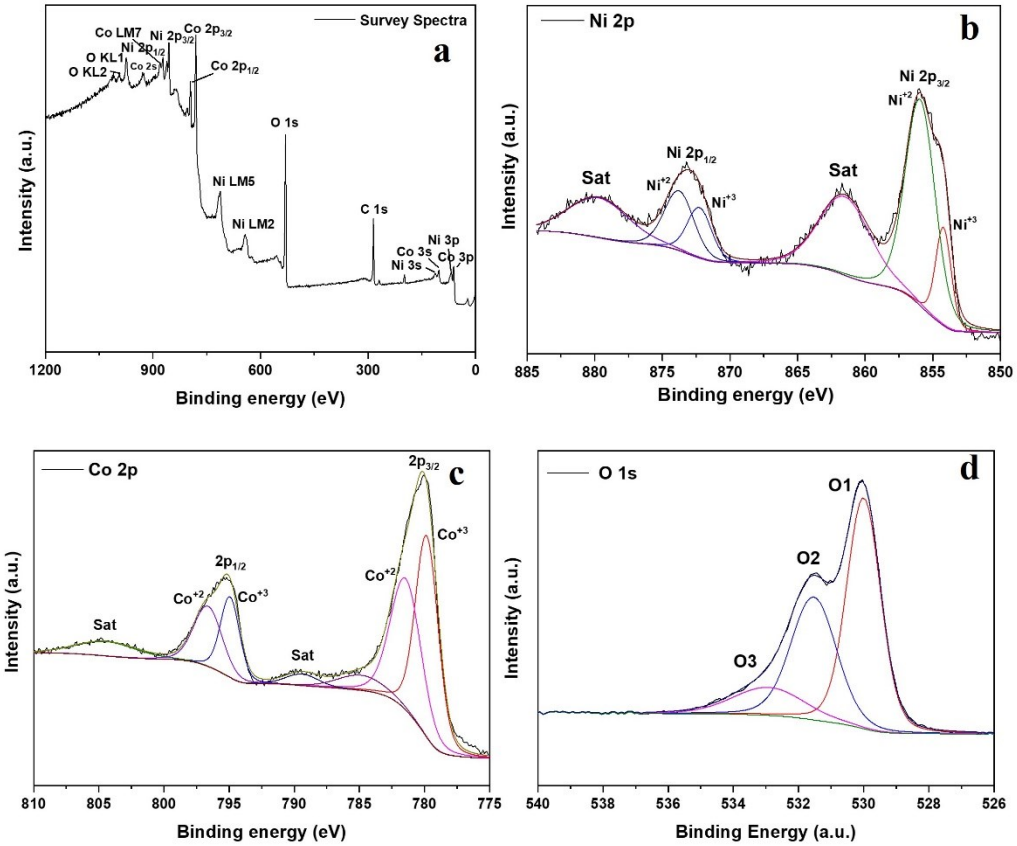

Figure S8: HER activity of other samples synthesized with various (a) amount of $RuCl_3$, (b) dipping time, and (c) calcination temperature

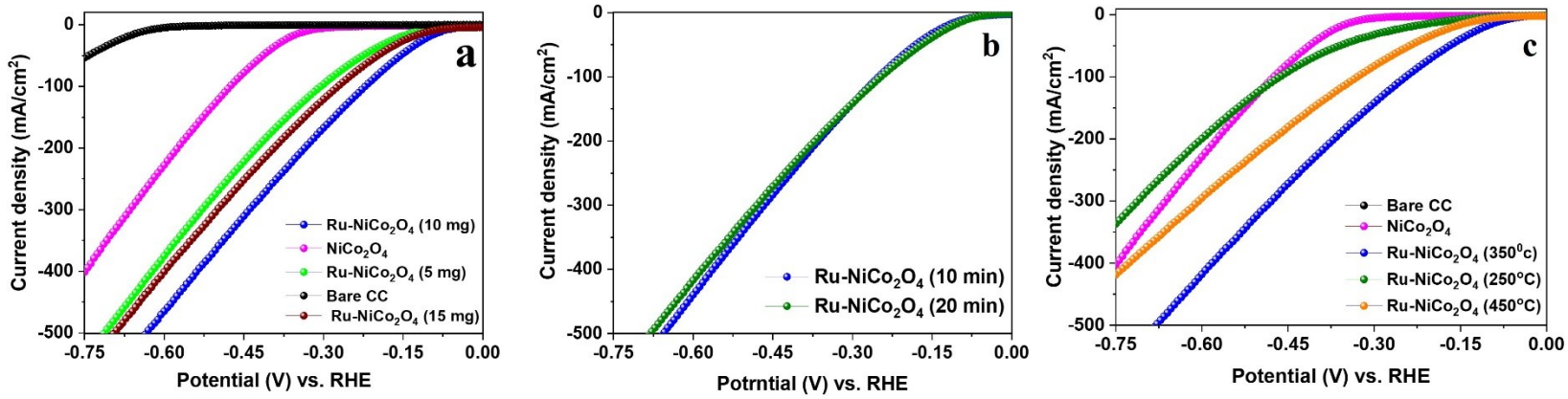

Figure S9: (a) CV analysis for Ru-SAC $NiCo_2O_4$, (b) $NiCo_2O_4$, ECSA analysis of (c) Ru-SAC $NiCo_2O_4$, and (d) $NiCo_2O_4$ sample

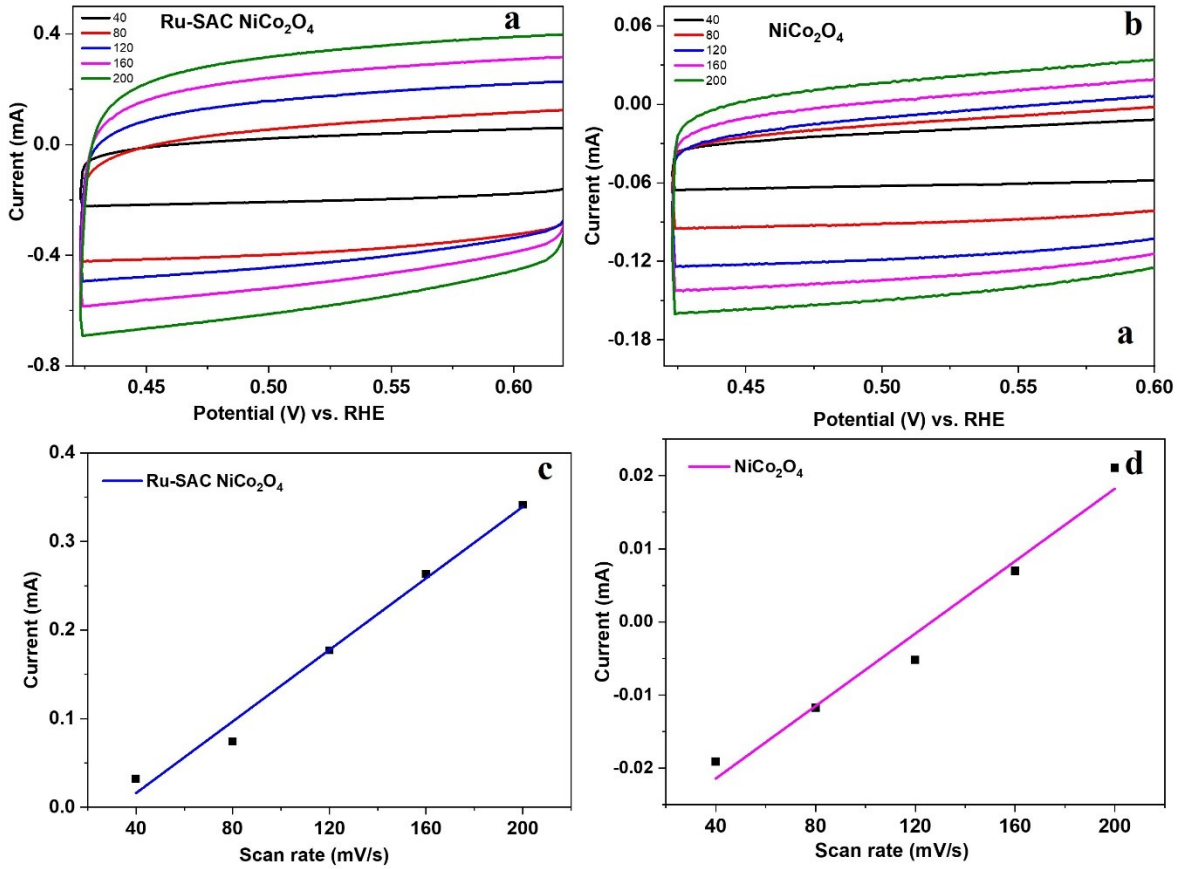

Figure S10: (a) CV analysis for pristine and Ru-SAC $NiCo_2O_4$ sample

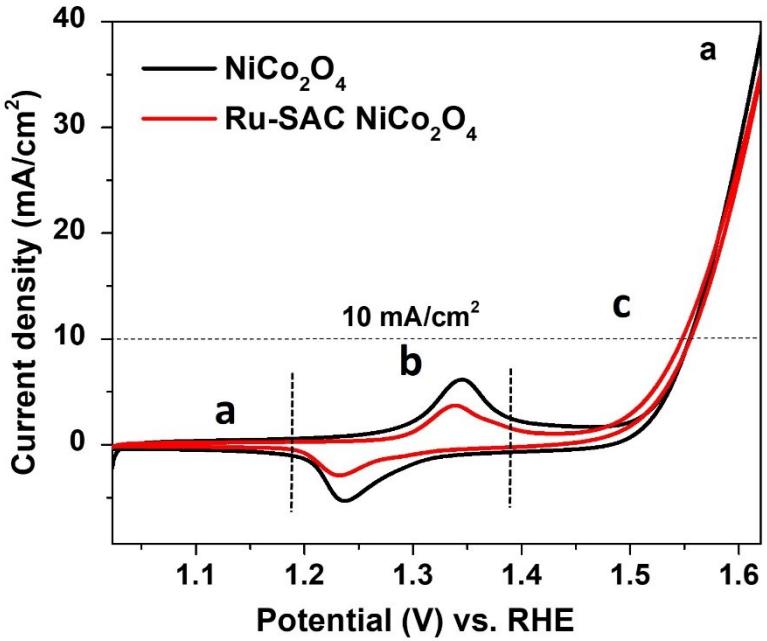

a: -OH + * ⟷ *OH;

b: 2 *OH + Ni^{+2} ⟷ Ni^{3+}—O* + H_2O;

c: Ni^{+3}—O* + $2OH^-$ ⟷ Ni^{3+}—O* + O_2

Figure S11: (a) LSV before and after 1000 cycle, (b) chronoamperometric data of Ru-SAC $NiCo_2O_4$ for OER.

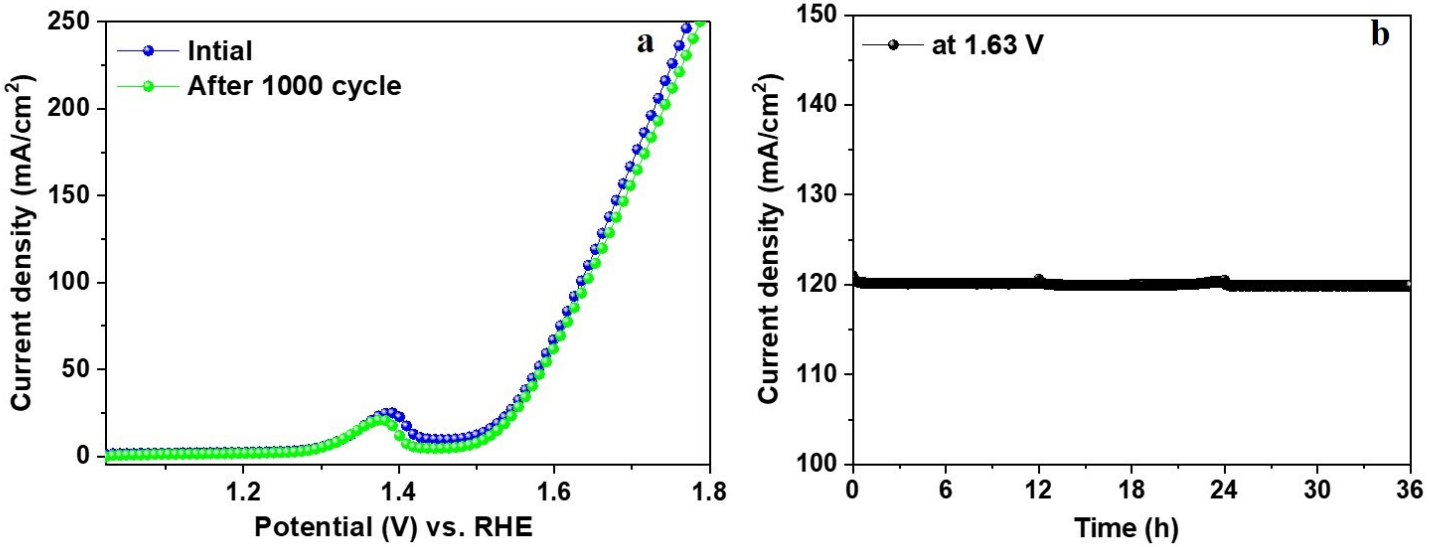

Figure S12: Post electrocatalysis (a) FESEM and (b) XRD analysis of Ru-SAC $NiCo_2O_4$

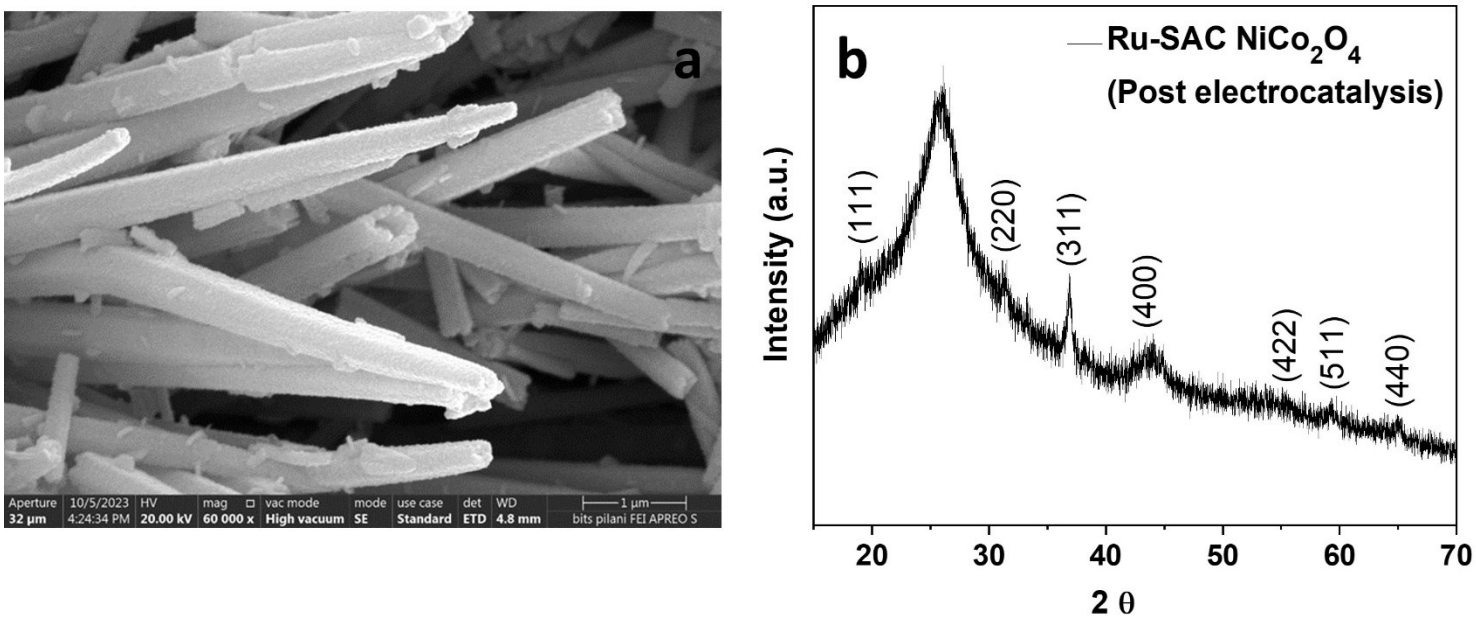

Figure S13: Post electrocatalysis XPS analysis of Ru-SAC $NiCo_2O_4$ (a) survey spectra, deconvoluted spectra of (b) Ni 2p, (c) Co 2p, (d) Ru 3p, and (e) O 1s

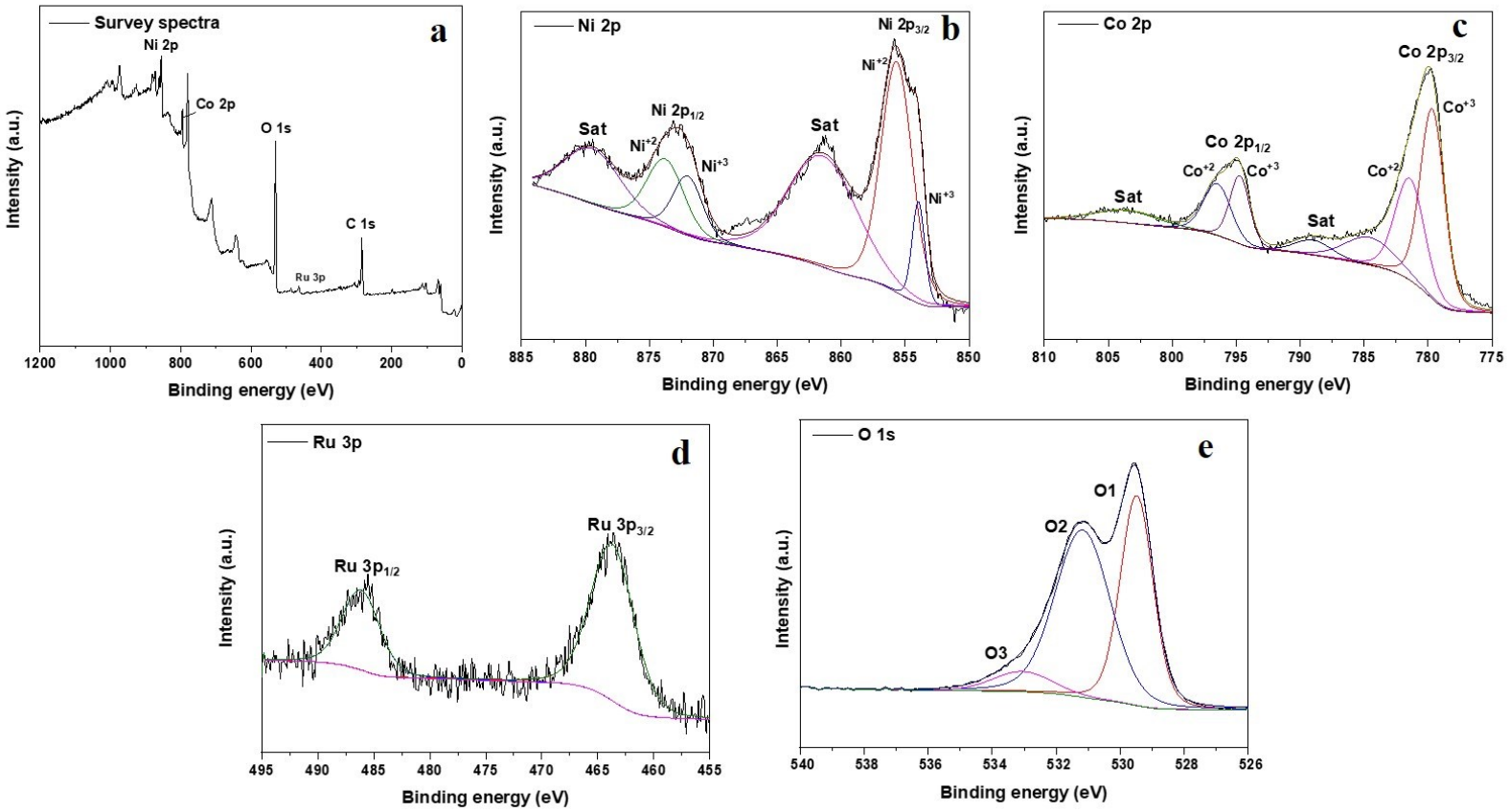

Figure S14: Comparative (a) LSV, and (b) EIS analysis for UOR of both $NiCo_2O_4$ and Ru-SAC $NiCo_2O_4$ sample. Inset of figure b shows the corresponding circuit.

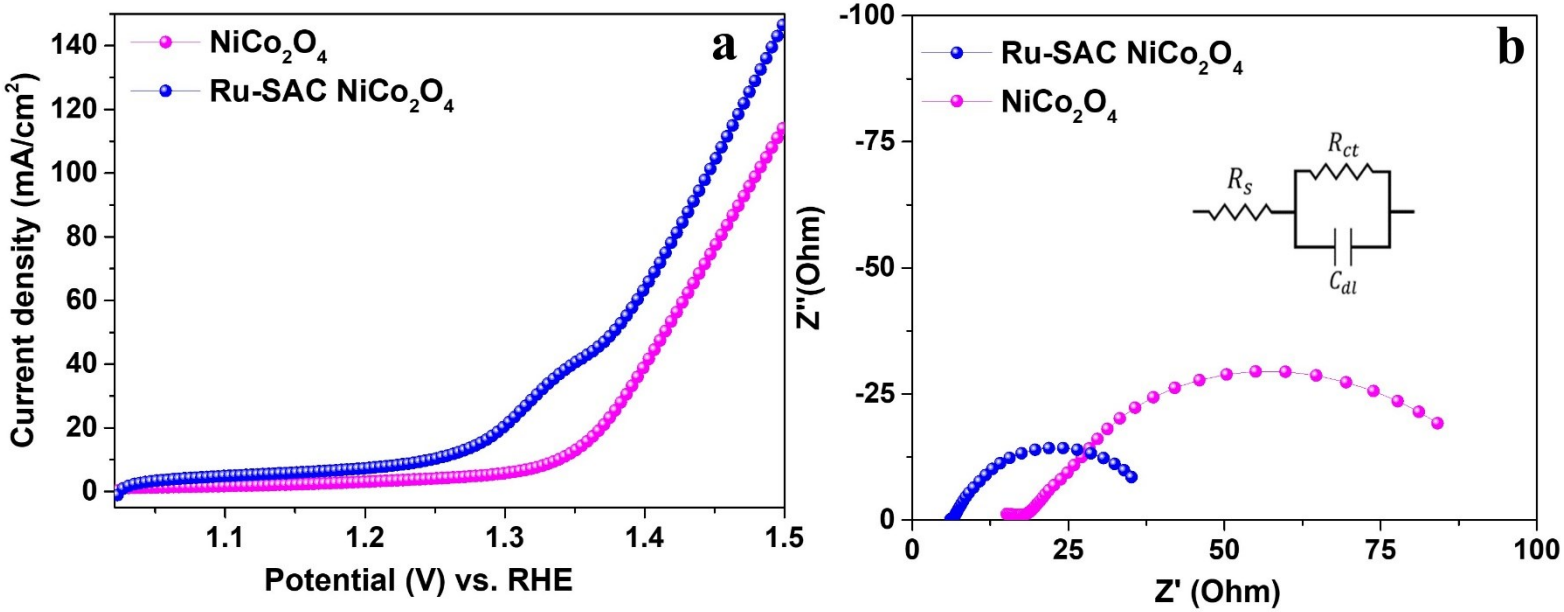

Figure S15: Optimized crystal structures for **(a)** (100), **(b)** (010) and **(c)** (001) planes of Ru-SAC $NiCo_2O_4$ compound.

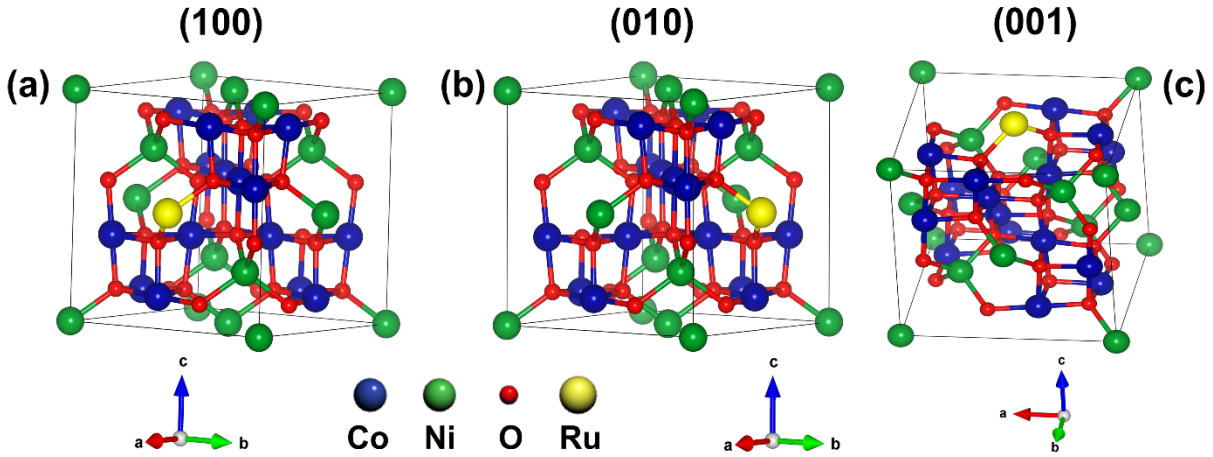

References:

[1] B. Ravel, M. Newville, *J. Synchrotron Radiat.* **2005**, 12, 537.

[2] B. Ravel, *J. Synchrotron Radiat.* **2001**, 8, 314.

[3] C. Shu, Y. Liang, Z. Zhang, B. Fang, *Eur. J. Inorg. Chem.* **2021**, 2021, 1659.

[4] C.-Z. Yuan, S. Wang, K. San Hui, K. Wang, J. Li, H. Gao, C. Zha, X. Zhang, D. A. Dinh, X.-L. Wu, Z. Tang, J. Wan, Z. Shao, K. N. Hui, *ACS Catal.* **2023**, 13, 2462.

[5] P. Li, M. Wang, X. Duan, L. Zheng, X. Cheng, Y. Zhang, Y. Kuang, Y. Li, Q. Ma, Z. Feng, W. Liu, X. Sun, *Nat. Commun.* **2019**, 10, 1711.

[6] J. Yin, J. Jin, M. Lu, B. Huang, H. Zhang, Y. Peng, P. Xi, C.-H. Yan, *J. Am. Chem. Soc.* **2020**, 142, 18378.

[7] J. Shan, C. Ye, S. Chen, T. Sun, Y. Jiao, L. Liu, C. Zhu, L. Song, Y. Han, M. Jaroniec, Y. Zhu, Y. Zheng, S.-Z. Qiao, *J. Am. Chem. Soc.* **2021**, 143, 5201.

[8] D. Wang, Q. Li, C. Han, Z. Xing, X. Yang, *Appl. Catal., B: Environmental* **2019**, 249, 91.

[9] P. Kuang, Y. Wang, B. Zhu, F. Xia, C.-W. Tung, J. Wu, H. M. Chen, J. Yu, *Adv. Mater.* **2021**, 33, 2008599.

[10] T. Li, S. Ren, C. Zhang, L. Qiao, J. Wu, P. He, J. Lin, Y. Liu, Z. Fu, Q. Zhu, W. Pan, B. Wang, Z. Chen, *J. Chem. Eng.* **2023**, 458, 141435.

[11] D. Cao, Z. Zhang, Y. Cui, R. Zhang, L. Zhang, J. Zeng, D. Cheng, *Angew. Chem. Int. Ed.* **2023**, 62, e202214259.